PPPL-2514

UC-427

PPPL-2514

ORBIT EFFECTS ON IMPURITY TR SPORT IN A ROTATING TOKAMAK PLA A

By

K.L. Wong and C.Z. Cheng

MAY 1988

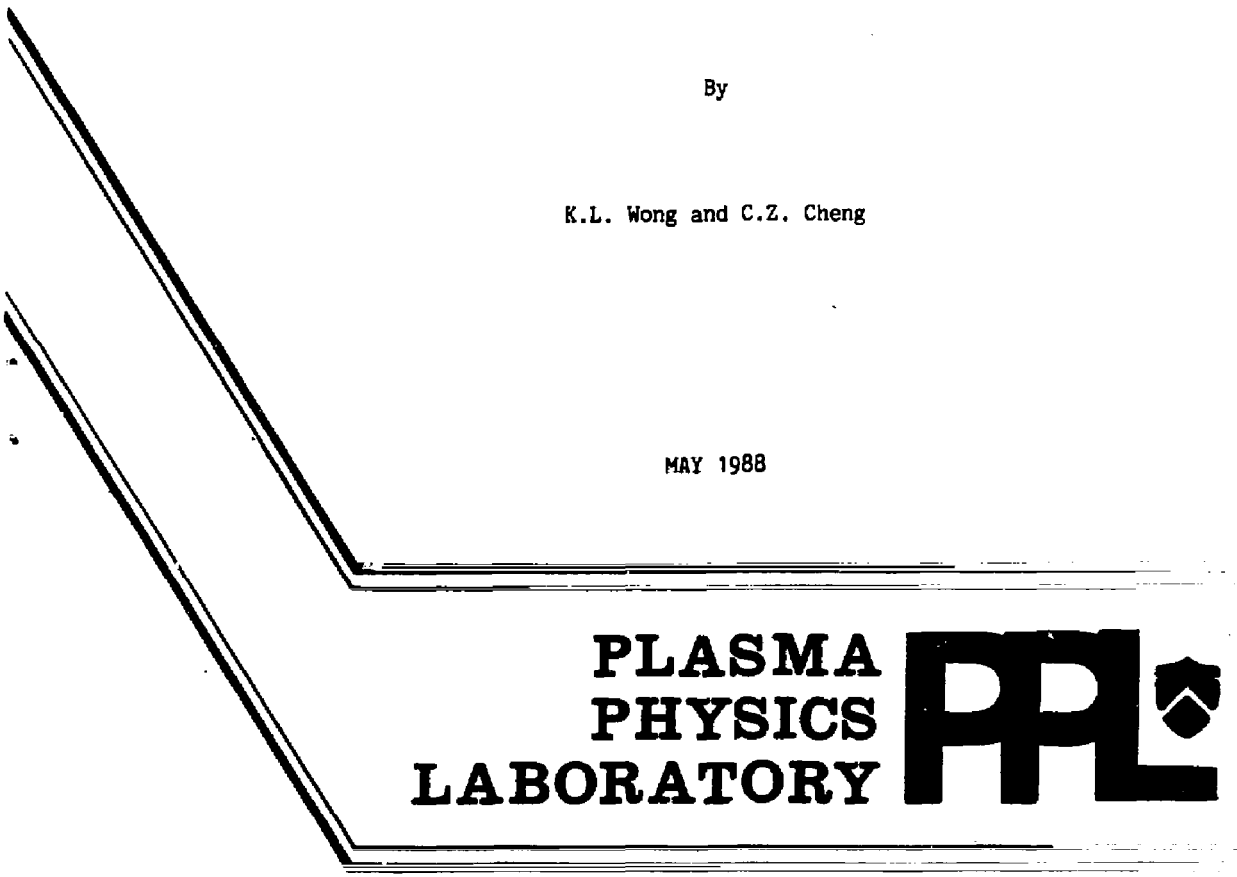

PRINCETON UNIVERSITY
PRINCETON, NEW JERSEY

PREPARED FOR THE U.S. DEPARTMENT OF ENERGY,
UNDER CONTRACT DE-AC02-76-CHO-3073.

ORBIT EFFECTS ON IMPURITY TRANSPORT IN A ROTATING TOKAMAK PLASMA

PPPL--2514

DE88 011167

K.L. Wong and C.Z. Cheng

Princeton Plasma Physics Laboratory

Princeton, New Jersey 08543

Abstract

Particle orbits in a rotating tokamak plasma are calculated from the equation of motion in the frame that rotates with the plasma. It is found that heavy particles in a rotating plasma can drift away from magnetic surfaces significantly faster with a higher bounce frequency, resulting in a diffusion coefficient much larger than that for a stationary plasma. Particle orbits near the surface of a rotating tokamak are also analyzed. Orbit effects indicate that more impurities can penetrate into a plasma rotating with counter-beam injection. Particle simulation is carried out with realistic experimental parameters and the results are in qualitative agreement with some experimental observations in the Tokamak Fusion Test Reactor (TFTR).

I. Introduction

Impurity control is an important topic in magnetic fusion research. Heavy impurities in tokamak plasmas can degrade the energy confinement, alter the current density profile, dilute the fusion fuel concentration and reduce the fusion power output. All these adverse effects ought to be kept to a minimum in a fusion reactor. Impurity control by an external momentum source, like neutral beam injection, has been under investigation for many years. Some theories[1,2] predict that impurity convection in tokamaks can be controlled by the direction of neutral beam injection with respect to the plasma current. Co-injection produces outward impurity convection and counter-injection produces inward convection. This kind of impurity behavior was observed in the ISX-B tokamak[3]: co-injection tended to drive impurities out of the plasma while counter-injection caused impurity accumulation in the plasma core until the plasma disrupted. However, these effects were not observed in the Princeton Large Torus (PLT). Impurity injection experiments on PLT[4] showed no significant difference in impurity transport with co- or counter-beams: the temporal evolution of impurity line radiation was quite similar in both cases. The major difference was in the amount of impurity penetrating into the plasma interior. A given injected amount resulted in a larger impurity concentration in the core plasma with counter-beams than that with co-beams. Similar results were also obtained in the Tokamak Fusion Test Reactor (TFTR) recently.[5]

In 1985, very high ion temperature (~10 keV) plasmas were first produced in TFTR with co-beams injecting into a low current (~800 kA), low density plasma. This mode of operation is called the energetic ion mode [6] in which the plasma rotates at very high speed ($\lesssim 10^8$ cm/sec). In these experiments, the ion temperature was measured by Doppler broadening of line radiation from

heavy impurities (Ti XXI) in the plasma.[7] When the plasma rotates at high speed, the heavy impurity concentration drops to a very low level. It then becomes difficult to measure the ion temperature with good temporal resolution because the lines are not bright enough. Sometimes, additional impurities are injected by the laser-blowoff technique to enhance the line brightness, but the injected particles leave the plasma very quickly when the plasma rotates at high speed. In order to fit the experimental data[8] on the temporal evolution of impurity line radiation, one has to include a large diffusion coefficient in the transport equations for the impurities. At low plasma currents, the diffusion coefficient is larger for plasmas rotating at high speed. Since existing theories[1,2] on impurity transport mainly emphasize rotation effects on impurity convection, the recent experimental observations in TFTR prompted us to investigate rotation effects on impurity diffusion. A self-consistent transport theory[9] was published recently for impurities in the banana regime and significant enhancement in the diffusion coefficient was found due to plasma rotation. It was pointed out in that paper[9] that the theory cannot be compared with experiments which are usually in the Pfirsch-Schlüter or plateau regime. In this paper, we attempt to explain some of the experimental observations from the orbits of impurity ions in a rotating plasma. The orbit calculation is formulated in Sec. II. Implications of the orbit characteristics and their relevance to experimental observations are presented in Sec. III. These results are substantiated by particle simulations described in Sec. IV. A summary is given in Sec. V. The analysis presented here is based on the experimental parameters in TFTR. MKS units are used in this paper except where otherwise specified.

II. Formulation

We consider a tokamak that has concentric circular magnetic surfaces. Each magnetic surface of minor radius r rotates as a rigid shell about the axis of symmetry with angular frequency $\omega(r)$. In a hot tokamak plasma, the electric conductivity is high enough such that magnetic field lines are frozen in and rotate with the plasma. We choose a toroidal coordinate system (see Fig. 1a) which rotates with the plasma in which the magnetic field lines are stationary. This technique has been used in a previous work[10] by other authors. The equation of motion for a charged particle with charge number Z in a rotating plasma is:

$$m \frac{d\vec{v}}{dt} = Ze (\vec{E} + \vec{v} \times \vec{B}) - 2 m \vec{\omega} \times \vec{v} - m \vec{\omega} \times [\vec{\omega} \times (\vec{R}_o + \vec{r})] \quad . \tag{1}$$

R_o is the plasma major radius and the three terms on the right-hand side of Eq. (1) are the Lorentz force, the Coriolis force, and the centrifugal force, respectively. Suppose the bulk plasma consists of electrons and a single ion species of mass m_i and charge number Z_i. We put Z_i equal to the plasma effective ion charge number Z_{eff} and $m_i = 2 Z_{eff} m_p$ where m_p is the proton mass. The magnetic surface is an equipotential surface in a stationary plasma, i.e., $\Phi = \Phi_o(r)$. In a rotating plasma, the ions are pushed towards the large-major-radius side by centrifugal force, which does not directly affect the electrons because of their small mass. This charge separation gives rise to a potential variation on the magnetic surface. Assume the electrons and ions have Boltzmann distributions:

$$n_e = N_e(r) \exp\left(\frac{e\Phi}{T_e}\right) \tag{2a}$$

$$n_i = N_i(r) \exp\left(\frac{-[Z_i e \Phi - (m_i/2)\omega^2 R^2]}{T_i}\right) \quad . \tag{2b}$$

Charge neutrality requires $n_e = Z_i n_i$ from which we can solve for the potential Φ and yield:

$$\Phi = \Phi_o(r) + \frac{m_i\omega^2}{2e} \frac{T_e}{T_i + Z_i T_e} (R^2 - \langle R^2 \rangle) \tag{3}$$

where $\langle\ \rangle$ denotes averaging over the magnetic surface. Equation (3) agrees with the result previously obtained by Hinton and Wong[10] when $Z_i = 1$.

Let m_I and Z_I denote the mass and charge number of the impurity ions whose density is very low such that their presence causes negligible changes in Z_{eff}, Φ and other plasma parameters. It has been shown[11] that the magnetic moment $\mu = (1/2)\, m_I v_\perp^2/B$ and the particle energy $\varepsilon = m_I v^2/2 + Z_I e\Phi - m_I\omega^2 R^2/2$ are adiabatic invariants in the rotating frame. Impurity ions at $R = R_1$ (see Fig. 1a) are trapped if $v_\parallel = 0$ before the particles reach $R = R_2$. This is equivalent to:

$$\frac{1}{2} m_I[v_\parallel^2 - (\frac{R_1}{R_2} - 1)v_\perp^2] < \frac{1}{2} m_I\omega^2(R_1^2 - R_2^2) + Z_I e\,[\Phi(R_2) - \Phi(R_1)] \quad . \tag{4}$$

The boundary between trapped and untrapped particles in velocity space is a hyperbolic surface as shown in Fig. 1b. Nearly all the heavy impurity ions are trapped when a plasma is rotating at high velocity like the energetic ion

mode plasma in TFTR.

Equation (1) can be solved by use of the guiding center approximation. The equations of motion for the guiding centers are given by:

$$\frac{d(\vec{R}_o+\vec{r})}{dt} = \vec{W} = \frac{\mu}{Z_I eB^2}\left(1+\frac{2\,v_\parallel^2}{v_\perp^2}\right)\vec{B}\times\vec{\nabla}B - \frac{2\,m_I[\vec{\omega}\times v_\parallel(\vec{B}/B)]\times\vec{B}}{Z_I eB^2}$$

$$- \frac{m_I\{\vec{\omega}\times[\vec{\omega}\times(\vec{R}_o+\vec{r})]\}\times\vec{B}}{Z_I eB^2} + \frac{\vec{E}\times\vec{B}}{B^2} + v_\parallel\frac{\vec{B}}{B} \qquad (5a)$$

$$\frac{dv_\parallel}{dt} = -\frac{\mu}{m_I}\frac{\vec{B}}{B}\cdot\vec{\nabla}B - \vec{\omega}\times[\vec{\omega}\times(\vec{R}_o+\vec{r})]\cdot\frac{\vec{B}}{B} + \frac{Z_I e}{m_I}\vec{E}\cdot\frac{\vec{B}}{B} \quad . \qquad (5b)$$

The first term in Eq. (5a) is the guiding center drift velocity due to the magnetic field gradient and field line curvature. The other terms are due to the Coriolis force, the centrifugal force, the electric field $\vec{E} = -\vec{\nabla}\Phi$, and the velocity parallel to the magnetic field. In the parameter regime of interest, the guiding center drift velocity $W_\perp$ is always much smaller than the thermal velocity. This allows us to drop some small terms of the order of $W_\perp/v_\perp$ when we derive Eq. (5b). Guiding center orbits can be obtained by integrating Eq. (5a) together with Eq. (5b). For typical energetic ion mode plasmas in TFTR, the banana widths of impurity ion orbits are about a few centimeters, which is only a small fraction of the minor radius (82 cm). Therefore, it is a reasonably good approximation to neglect the variation of

$\omega(r)$ along the particle orbit. For a more accurate treatment, variation of $\omega(r)$ can be accounted for by a velocity transformation when the particle moves from one magnetic surface to the other.

III. Orbit Effects

Collisionless particle orbits are obtained from Eqs. (1) and (5). We use the magnetic field for a circular cross section tokamak which has the following form:

$$B_\phi = \frac{R_o}{R} B_o \tag{6a}$$

$$B_\theta = \frac{B_o}{q(r)} \frac{r}{R} \quad , \tag{6b}$$

where $q(r) = q(0)\ (1 + r^2/r_c^2)$ is the safety factor of the flux surface at r. Typical TFTR parameters are used in the calculation: $R_o = 2.45$ m, $a = 0.82$ m, $r_c = 0.32$ m, $B_o = 4$-5 tesla, and $q(0)$ is chosen for plasma currents in the range of 0.7-1.1 MA, which is typical for energetic ion mode operation. In a stationary plasma, a banana orbit is almost symmetric with respect to the magnetic surface on which the reflection points lie. In other words, the maximum excursions (Δ_+ and Δ_-) from this magnetic surface are nearly the same on both sides of the orbit. A strong asymmetry develops in a rotating plasma. When a plasma rotates with co-injecting beams, the orbit excursion is larger on the outside. The opposite is true for counter-beam rotation. This orbit characteristic is schematically depicted on Fig. 2. It can be understood from the radial component of the drift velocity:

$$W_r = \frac{m_I}{Z_I eB}\left[-\omega^2 R + 2v_\parallel \omega - \left(\frac{v_\perp^2/2 + v_\parallel^2}{R}\right) + \frac{m_i}{m_I}\,\frac{Z_I T_e}{T_i + Z_i T_e}\,\omega^2 R\right] \sin\theta \quad . \tag{7}$$

The orbit asymmetry is caused by the second term on the right-hand side of Eq. (7), which comes from the Coriolis force. The sign of this term is determined by the sign of $v_{\parallel}$ as well as the direction of plasma rotation, i.e., the sign of ω. By integrating W_r over time along the trapped particle orbit, the banana asymmetry is estimated to be:

$$\Delta_+ - \Delta_- \simeq \frac{4m_I\omega}{Z_I e B_\theta} (1 - \cos\theta_o) r \simeq \frac{4\omega}{\Omega_\theta} (1 - \cos\theta_o) r \quad ,$$

where $\pm\theta_o$ are the poloidal angles of the reflection points, and Ω_θ is the impurity ion gyrofrequency in the poloidal magnetic field.

During impurity injection experiments, freshly ionized impurities near the plasma surface are essentially stationary in the laboratory frame and they are counter-rotating in the plasma frame with co-beam injection. Therefore, their first banana orbits bounce radially outward towards the limiter as depicted in Fig. 3. This can be verified from Eq. (7). At the first reflection point, $\sin\theta < 0$ for co-injection and $W_r > 0$, i.e., the particle bounce is radially outward. On the other hand, impurities injected into a rotating plasma with counter-beams have their first banana orbits bounce radially inward and, therefore, have a better chance to penetrate into the plasma interior. This orbit effect offers a qualitative explanation for the observation of higher impurity concentration in rotating plasmas with counter-beams.[4,5]

If one neglects the nonuniformity of the impurity ion density on a flux surface, the neoclassical diffusion coefficient of the impurity ions in the collisional regime can be estimated from the radial component of the drift velocity as follows:

$$D_{neo} = \lim_{\tau \to \infty} \frac{(\Delta r)^2}{2\tau} = \lim_{\tau \to \infty} \frac{1}{2\tau} \int_0^\tau dt \int_0^\tau dt' \, W_r(t) \, W_r(t') \quad . \tag{8}$$

The integrand in Eq. (8) can be written as:

$$W_r(t) \, W_r(t') = F \sin\theta \sin\theta' = \frac{F}{2} [\cos(\theta - \theta') + \cos(\theta + \theta')] \quad ,$$

where F contains variables $v_\perp$, $v_\parallel$, ω, etc. Consider particles doing a random walk[12] along magnetic field lines. The distance traveled along the field line is related to $\theta - \theta'$ via the rotational transform ι. If the collisional mean free path is much less than the plasma major radius, the impurity distribution function is locally Maxwellian with a temperature T_I the same as the bulk ion temperature. Equation (8) can then be evaluated to yield:

$$D_{neo} = \frac{1}{4} \left(\frac{m_I}{Z_I eB}\right)^2 \left[\omega^4 R^2 \left(1 - \frac{m_i}{m_I} \frac{Z_I T_e}{T_i + Z_i T_e}\right)^2 \right.$$

$$\left. + \omega^2 \left(1 - \frac{m_i}{m_I} \frac{Z_I T_e}{T_i + Z_i T_e}\right) \frac{4T_i}{m_I} + \frac{4T_i^2}{m_I^2 R^2} \right] \frac{m_I \nu}{T_i} R^2 q^2 \quad , \tag{9}$$

where ν is the impurity ion collision frequency and q is the safety factor ($q = 2\pi/\iota$). In a stationary plasma, $\omega = 0$ and Eq. (9) is reduced to the same result as obtained by Galeev and Sagdeev.[13] When $m_I \omega^2 R^2 > T_i$, the diffusion coefficient becomes significantly larger. It should be noted that this is not a self-consistent calculation and one should be aware of the limitations of Eq. (9). For particles near $\theta = \pm\pi/2$, W_r is larger in magnitude and maintains the same sign for a longer period of time when compared with particles near

$\theta = 0$ or $\theta = \pi$. Due to the influence of the centrifugal force, the impurity ion density $n_I(\theta)$ is not uniform on a flux surface. $n_I(\theta)$ should have a Boltzmann distribution given by:

$$n_I(\theta) = N_I \exp\left[-\left(\frac{Z_I e\Phi}{T_I} - \frac{m_I}{2}\frac{\omega^2 R^2}{T_I}\right)\right] \quad .$$

It peaks at $\theta = 0$ and Equation (9) tends to overestimate the diffusion coefficient. When ω is not very large, the increase in $n_I(0)$ is mainly due to the drop in $n_I(\pi)$ without a large change in $n_I(\pi/2)$, and its effect on D_{neo} is small. When ω is very large such that $n_I(0) + n_I(\pi) >> 2n_I(\pi/2)$, then the error becomes significant and Eq. (9) should be properly weighted by the impurity density distribution. Another assumption which can break down at high values of ω is the constant step size of the random walk process along the magnetic field line. Particles moving towards $\theta = 0$ have step sizes larger than those moving away from $\theta = 0$ because of the centrifugal force, and this difference can be significant when ω is very large. All these complications will be properly taken into account by the particle simulation method presented in the next section.

The above result applies only to impurity ions in the Pfirsh-Schlüter regime. In the TFTR energetic ion mode plasma, impurity ions are collisional only at the edge. They are mildly collisionless near the plasma core and the ions no longer have a Maxwellian velocity distribution. Instead of solving the drift kinetic equation, we can obtain some physical insight from the properties of the particle orbits. Figure 4 shows that for particles trapped between fixed poloidal angles, the banana width Δ_b and the bounce frequency ω_B increase with ω. When $(1/2)\, m_I\, \omega^2 R^2 > T_I$, Δ_b is approximately proportional to ω/q. However, for particles with the same velocity in the plasma frame at

$\theta = 0$, Δ_b is not sensitive to ω, and ω_B increases almost linearly with ω as shown in Fig. 5. In fact, the variation of the banana width can be estimated analytically; $\Delta_b = 2\, v_\parallel(\theta=0)/\Omega_\theta$ which is in good agreement with the numerical results present in Fig. 4 and Fig. 5. The diffusion coefficient in the banana regime can be roughly estimated by $D_{neo} = f_T \nu_{eff} \bar{\Delta}_b^2$ where f_T is the fraction of trapped particles. ν_{eff} is the effective collision frequency for the orbit of an "average" trapped particle to shift one banana width $\bar{\Delta}_b$. In a stationary plasma, $f_T \sim (r/R_o)^{1/2}$, $\nu_{eff} \sim (R_o/r)\nu$ where ν is the 90° pitch-angle scattering frequency mainly due to Coulomb collisions with the bulk ions in the plasma. Let $\bar{\Delta}_b = \Delta_o$ in a stationary plasma, then, $D_{neo} \sim (R_o/r)^{1/2}\, \nu\, \Delta_o^2$. In a rapidly rotating plasma, $f_T \sim 1$, $\nu_{eff} \sim 1.27\, \nu$ which is the collision frequency for $v_\parallel$ to change sign, $\bar{\Delta}_b = \Delta_\omega$, and $D_{neo} \sim 1.27\, \nu\, \Delta_\omega^2$. Previous work by S.K. Wong[9] shows that in the banana regime, there is a significant enhancement in D_{neo} due to plasma rotation. This is primarily because Δ_ω^2 is significantly larger than Δ_o^2. The situation is more complicated in the TFTR experiments because the impurity ions are not in the banana regime when the plasma is stationary, i.e., $\nu_{eff} \sim (R_o/r)\, \nu > \omega_B$. When the plasma is rotating at high velocity, ν_{eff} becomes smaller and ω_B becomes significantly larger. Therefore, the banana regime extends to a higher collision frequency. In other words, impurity ions in the plateau or Pfirsch-Schlüter regime when the plasma is stationary can get into the banana regime in a rotating plasma with the same plasma parameters, provided that ω is large enough. The transition into the banana regime is accompanied by a large enhancement in the diffusion coefficient. Figure 6 illustrates this effect of plasma rotation on the diffusion coefficient. For the TFTR energetic ion mode plasmas, $\omega_B \gtrsim \nu_{eff}$, i.e., the impurity ions are near the transition region between the banana and the plateau regimes. One would expect an order of

magnitude enhancement in D_{neo} from the orbit effect. This will be substantiated by particle simulation results presented in the next section.

IV. Particle Simulation

A toroidal particle simulation code[14] is employed to investigate the impurity transport. The code follows the impurity guiding center positions by integrating Eq. (5). The particle orbit integration is carried out by the second order predictor-corrector method with the following time stepping scheme:

$$\vec{r}'_{n+1} = \vec{r}_{n-1} + 2\,\Delta t\,\vec{W}\,(\vec{r}_n, t_n)$$

$$\vec{r}_{n+1} = \vec{r}_n + \frac{\Delta t}{2}\left[\vec{W}\,(\vec{r}_n, t_n) + \vec{W}\,(\vec{r}'_{n+1}, t_{n+1})\right] \quad . \tag{10}$$

When a particle moves from one flux surface to the next, $v_\parallel$ is properly adjusted in order to account for the shear in the plasma rotation velocity. The initial impurity particle positions are loaded according to the distribution

$$f\,(r,\theta,\phi) = g\,(r)\,\exp\left[-\frac{(\theta-\theta_o)^2}{(\Delta\theta)^2} - \frac{(\phi-\phi_o)^2}{(\Delta\phi)^2}\right] \quad , \tag{11}$$

where g(r) is the radial distribution and a periodicity constraint is imposed on θ and ϕ. Pitch angle scattering is modeled by a Monte-Carlo collision operator.[15] The velocity of each impurity particle is scattered by the bulk ions in each time step Δt with a change in pitch angle $\theta_v = \cos^{-1}(v_\parallel/v)$ given by

$$\Delta\theta_v = [-4\,\nu_\perp^{Ii}\,\Delta t\,\ell n(1-\alpha)]^{1/2} \quad , \tag{12}$$

where α is a random number between 0 and 1. The 90° pitch angle collision frequency is taken to be

$$\nu_\perp^{Ii} = 1.4 \times 10^{-7}\, Z_I^2 n_i Z_{eff}^2 \lambda_{Ii}\, (2\, Z_{eff} T_i)^{1/2} m_p/(m_I \varepsilon_I)\ \text{sec}^{-1} \quad . \tag{13}$$

We assume a single bulk ion species of mass m_i and charge number Z_{eff}. T_i is the bulk ion temperature in eV, ε_I is the individual impurity ion kinetic energy in eV, λ_{Ii} is the Coulomb logarithm taken to be 15. The other quantities are in cgs units. For impurity transport studies, we place 1024 impurity particles on a flux surface at t = 0 with $T_I = T_i$. The initial angular distribution (θ-dependence) of these particles is chosen to be close to the Boltzmann distribution at equilibrium. This tends to speed up the convergence process when we calculate the diffusion coefficient. The guiding center positions of these particles are calculated as a function of time and the diffusion coefficient is calculated from

$$D_{neo} = \frac{[\langle(\Delta r)^2\rangle_p - \langle\Delta r\rangle_p^2]}{2t} \quad , \tag{14}$$

where Δr is the excursion of a particle from the original flux surface and $\langle\rangle_p$ denotes averaging over all the particles. The purpose of the second term in Eq. (14) is to eliminate contributions from particle convection. In order to compare with experiments in TFTR, we choose either germanium or iron as the impurity species. The charge number Z_I is determined by the local electron temperature and the ionization potential $\Phi_I(Z)$: $Z_I = Z$ if $\Phi_I(Z) < T_e \leq \Phi_I$

(Z + 1). Lorentzian plasma parameter profiles are used for computational convenience:

$$n_e(r) = n_e(0)\ (1 + 4r^2/a^2)^{-1}$$

$$T_e(r) = T_e(0)\ (1 + 9r^2/a^2)^{-1}$$

$$T_i(r) = T_I(0)\ (1 + 9r^2/a^2)^{-1} \qquad (15)$$

$$\omega(r) = \omega(0)\ (1 + 4r^2/a^2)^{-1}$$

$$B_o = 40\ \text{kG},\ R_o = 245\ \text{cm},\ a = 82\ \text{cm},\ Z_{eff} = 4.0\ .$$

We put the zeroth order radial electric field to be $E_r = 400/(1 + 17\ r^2/a^2)$ volts/m, and the safety factor to be $q(r) = 1.1\ (1 + 6.5455\ r^2/a^2)$, which corresponds to 700 kA of plasma current. The central parameters are chosen to be similar to the experimental values: $n_e(0) = 2 \times 10^{13}\text{cm}^{-3}$, $T_e(0) = 4$ keV, $T_i(0) = 10$ keV, $\omega(0) = 2 \times 10^5$ rad/sec. Figure 7 shows the spread of the 1024 particle guiding centers initially located at r = a/2. In order to determine the diffusion coefficient, we plot $\Delta^2 \equiv (1/2)\ [\langle(\Delta r)^2\rangle_p - \langle\Delta r\rangle_p^2]$ versus time as depicted on Fig. 8. After a couple of collisions (90° pitch angle scattering), Δ^2 increases linearly with time and the slope of the linear portion is the diffusion coefficient. This procedure is the same as that employed by Tsang et al.[16] At t = 0, the particles are loaded with the spatial distribution given in Eq. (11). In order to simulate the Boltzmann distribution at equilibrium, we choose $\Delta\theta = [\{m_I - m_i Z_I T_e/(T_i + Z_i T_e)\}\ \omega^2 R_o r/2T_i]^{-1/2}$. For our plasma parameters, $\Delta\theta \geq 1$ radian. The diffusion

coefficient converges to a fixed value very quickly while the excursion from the original flux surface is small ($\Delta r \ll a$). There is no need to include energy equilibration between the impurity ions and the bulk ions because the impurity ions are loaded with a temperature equal to the local bulk ion temperature. The results obtained this way are approximately a factor of two lower than the preliminary results published previously,[17] and we believe that the results presented here are more accurate because we have successfully eliminated the slow convergence problem primarily caused by the energy equilibriation process. Figure 9 compares the diffusion coefficient for a rotating plasma with that for a stationary plasma. It is apparent that neoclassical diffusion is enhanced by more than an order of magnitude as a result of plasma rotation. This substantiates the heuristic argument based on particle orbit characteristics presented in Sec. III. In a stationary plasma, the impurity ions are collisional, D_{neo} is very small, and impurity transport is governed by some anomalous processes. In the rotating plasma, the impurity ions are in the banana regime. D_{neo} can be large enough to compete with anomalous transport and causes enhanced diffusion in impurity injection experiments. Figure 10 shows the variation of D_{neo} with the plasma current at two different rotation velocities. The shape of the current density profile and other plasma parameters remain the same. D_{neo} is obtained by particle simulation at $r = a/2$. The results show that at high rotation velocity, D_{neo} is approximately proportional to I_p^{-2}. It drops to a low value at high plasma current and low rotation velocity, at which we expect that impurity transport would be dominated by other anomalous processes. In other words, neoclassical diffusion can surface only in a low current plasma rotating at high speed, such as the energetic ion mode plasma in TFTR. This qualitatively agrees with the observations reported previously.[8] Quantitative comparison with

experiment is not possible at this time due to the lack of profile data on $\omega(r)$, $T_i(r)$, and $\Phi_o(r)$.

In order to investigate the variation of D_{neo} with collision frequency, we evaluate D_{neo} at r = a/2 and vary the plasma density while other plasma parameters remain the same. The result is shown in Fig. 11. The impurity ions are in the banana regime for $\nu \leq 10^4$ sec^{-1}. When the plasma is rotating at high speed, the transition from the collisionless regime to the collisional regime occurs at a collision frequency significantly higher than that when the plasma is stationary. This is because of the higher bounce frequency and lower ν_{eff} of the trapped particles in a rotating plasma as explained in Sec. III. D_{neo} is larger in a rotating plasma by at least an order of magnitude over the entire range of collision frequency shown in Fig. 11. At $\nu = 7.1 \times 10^4$ sec^{-1}, the impurity ions are in the Pfirsh-Schlüter regime. Particle simulation yields $D_{neo} = 3 \times 10^4$ cm^2/sec while Eq. (9) gives a value of 5.8×10^4 cm^2/sec. The discrepancy is primarily due to the nonuniform impurity density on the flux surface as explained previously. For a stationary plasma with the same parameters, Eq. (9) gives $D_{neo} = 1.8 \times 10^3$cm^2/sec which is in very good agreement with the particle simulation result of 1.9×10^3 cm^2/sec.

The variation of diffusion coefficient with rotation velocity is shown in Fig. 12. D_{neo} was evaluated at r = a/2 while $\omega(0)$ was varied with the same values of $T_i(r)$, $T_e(r)$, $n_e(r)$, and $\omega(r)/\omega(0)$. Within the range of our investigation, D_{neo} increases monotonically with ω. The impurity ions are in the banana regime for $\omega(0) \geq 2 \times 10^5$ rad/sec. In the banana regime, D_{neo} is approximately proportional to ω^2 in the range of ω shown in Fig. 12. This behavior is consistent with the results obtained previously.[9]

During impurity injection experiments, neutral impurity particles are injected onto the plasma surface by the laser blow-off technique. The

temperature of these neutral particles are much lower than the plasma ion temperature. After they are ionized, they will be heated up to the local ion temperature via Coulomb collisions. The macroscopic thermal equilibration between the background ions and the impurity ions is described by:

$$\frac{d}{dt} T_I = \bar{\nu}_{Ii} (T_i - T_I) \tag{16}$$

$$\bar{\nu}_{Ii} = \frac{1.8\times10^{-19} (m_I m_i)^{1/2} Z^2 Z_{eff}^2 n_i \lambda_{Ii}}{(m_I T_i + m_i T_I)^{3/2}} \text{ sec}^{-1} \quad , \tag{17}$$

where T_i and T_I are in eV and the other quantities are in cgs units. In order to include the energy equilibration process in the particle simulation code, we describe the relaxation of the impurity particle kinetic energy by:

$$\frac{d}{dt} \epsilon_I = \nu_{Ii} (\epsilon_i - \epsilon_I) \quad , \tag{18}$$

where ϵ_i and ϵ_I are the kinetic energy of the colliding background ion and the impurity particles, respectively. ν_{Ii} is the same as $\bar{\nu}_{Ii}$ given in Eq. (17) except T_I is replaced by ϵ_I. In Eq. (18), ϵ_i is picked by a generating function which represents the bulk ion Maxwellian velocity distribution. If we ensemble average Eq. (18) over the Maxwellian distributions of both ion species, Eq. (18) would reduce to Eq. (16).

For each time step Δt, Eq. (18) is integrated by the finite difference scheme:

$$\varepsilon_I^{n+1} = \varepsilon_I^n + \nu_{Ii}^n \Delta t(\varepsilon_i^n - \varepsilon_I^n) \quad . \tag{19}$$

This thermal equilibration scheme was tested with 1024 particles. The average kinetic energy of the impurity ions was found to approach T_i as expected, but the impurity ion velocity distribution becomes squarelike rather than Maxwellian. Therefore, this is not a perfect scheme. Nevertheless, it retains the essential feature of the energy equilibration process and it is employed in the particle simulation code to investigate impurity penetration through the plasma edge.

We follow the guiding center position of 3072 particles near the plasma edge. The limiters on TFTR are simulated by the following boundary condition: a particle is permanently removed from the plasma if

(a) $r > 81.2$ cm, and

(b) $1.1 \leq \phi \leq 1.5$, and

(c) $0.9 \leq \theta \leq 1.4$ or $-0.9 \geq \theta \geq -1.4$.

In the experiment, the impurity injector is located near $\theta \approx 0$ and impurity neutrals can only penetrate the plasma a few millimeters before they are ionized. Therefore, we start the ions at $r = 80.6$ cm (0.6 cm from the limiter radius) with an angular distribution $\exp(-\theta^2)\exp(-\phi^2)$. The initial velocity distribution is a non-drifting Maxwellian in the laboratory frame with a thermal velocity 5×10^5 cm/sec. Projection of the guiding center positions are shown in Fig. 13a. The particles drift across the magnetic field and spread out as shown in Fig. 13b and Fig. 13c. The particles that strike the

limiter are permanently removed from the plasma. Those particles outside the plasma boundary may re-enter the plasma before hitting the limiter. Careful inspection of Fig. 13b and Fig. 13c reveals that in addition to the density peaking at the large-major-radius side, there is also an up-down asymmetry. On the lower half-plane, there are more particles and they are located at a slightly larger minor-radius position. We note that the guiding center drift velocity points downward in this case. This asymmetry is reversed if we change the direction of the toroidal magnetic field so that the impurity ions drift upward. In a highly collisional plasma, the impurity ions can no longer move freely along magnetic field lines. They stay on the lower or upper half plane for a long period of time and the up-down asymmetry becomes very strong as shown in Fig. 14. This may be related to the experimental observations in Alcator[18] and ASDEX[19]. Figure 15 depicts the number of remaining particles versus time for co- and counter-injection cases. At the beginning, the rate of particle loss is much faster for co-injection than for counter-injection. After many collisions ($t > 3$ ms), the loss rates become comparable, and more particles remain in the plasma with counter-injection. In addition, these particles penetrate deeper into the plasma interior when compared with the case of co-injection. These differences are due to the orbit characteristics as explained in Sec. III. They offer a qualitative explanation for the observations in PLT[4] and TFTR[5] where more impurity ions can penetrate into the plasma interior with counter-injection. However, it should be pointed out that a finite rotation velocity at the plasma edge is necessary for the orbit effects to play an important role. A quantitative comparison with experimental data cannot be made because plasma parameters at the tokamak edge are very difficult to quantify.

V. Summary

In this paper, we calculate the orbits of impurity ions in a rotating plasma based on the guiding center approximation. At high rotation velocities, heavy impurity ions can drift significantly faster than in a stationary plasma and the trapped ions have larger banana width and higher bounce frequency. These orbit effects give rise to a significant enhancement in the particle diffusion coefficient. By use of a particle simulation code, we evaluate the neoclassical diffusion coefficient for heavy impurity ions in the energetic ion mode plasma in TFTR and find that its value is not far from what is needed to fit the experimental data at low plasma current.[8] Its variation with plasma current and rotation velocity is also consistent with experimental observations. From these results, one can expect that transport of the energetic α-particles in a tokamak reactor is likely to be neoclassical because of their large drift velocities. The orbit of a neutral particle entering a rotating plasma is also analyzed. When the particle is scattered from a passing orbit into a banana orbit, it bounces radially outward in a co-rotating plasma and radially inward in a counter-rotating plasma. This orbit effect can account for the difference in impurity concentrations during impurity injection into co-rotating and counter-rotating plasmas in PLT[4] and TFTR.[5] Qualitative agreement is obtained between particle simulation and experimental observations in TFTR.

ACKNOWLEDGMENTS

The authors wish to thank Dr. M. Bitter, Dr. S. Cowley, Dr. R.J. Goldston, Dr. R.J. Hawryluk, Dr. K. Hill, Dr. H. Hsuan, Dr. R. Hulse, Dr. A. Ramsey, Dr. J. Strachan, Dr. B. Stratton, Dr. S. Suckewer, Dr. S. von Goeler, and Dr. M. Zarnstorff for many helpful discussions. This work is supported by U.S. Department of Energy Contract No. DE-AC02-76-CH03073.

REFERENCES

[1]W.M. Stacey and D.J. Sigmar, Nucl. Fusion 19, 1665 (1979).

[2]K.H. Burrell, T. Ohkawa, and S.K. Wong, Phys. Rev. Lett. 47, 511 (1981).

[3]R.C. Isler et al., Phys. Rev. Lett. 47, 649 (1981).

[4]S. Suckewer et al., Nucl. Fusion 24, 815 (1984).

[5]K.L. Wong, C.Z. Cheng, B.C. Stratton, and A. Ramsey, in Proceedings of the Fourteenth European Conference on Controlled Fusion and Plasma Heating, Madrid, Spain, June 22-26, 1987, paper A-20.

[6]M. Murakami et al., Plasma Phys. Controlled Fusion 28, 17 (1986).

[7]M. Bitter et al., Phys. Rev. A 32, 3011 (1985).

[8]B.C. Stratton et al., J. Nucl. Mater. 145-147, 582 (1987).

[9]S.K. Wong, Phys. Fluids 30, 818 (1987).

[10]F.L. Hinton and S.K. Wong, Phys. Fluids 28, 3082 (1985).

[11]S.C. Cowley and C.M. Bishop, Culham Laboratory, Report No. CLM-M109, 1986 (unpublished).

[12]S. Chandrasekhar, Rev. Mod. Phys. 15, 3 (1943).

[13]A.A. Galeev and R.Z. Sagdeev, Zh. Eksp. Teor. Fig. 53, 348 (1967) [Sov. Phys. JETP 26, 233 (1968)].

[14]C.Z. Cheng and H. Okuda, J. Comput. Phys. 25, 133 (1977).

[15]R. Shanny, J.M. Dawson, and J.M. Greene, Phys. Fluids 10, 1281 (1967).

[16]K.T. Tsang, Y. Matsuda, and H. Okuda, Phys. Fluids 18, 1282, (1975).

[17]K.L. Wong and C.Z. Cheng, Phys. Rev. Lett. 59, 2643 (1987).

[18]J.L. Terry, E.S. Marmar, K.I. Chen, and H.W. Moos, Phys. Rev. Lett. 39, 1615 (1977).

[19]P. Smeulders, Nucl. Fusion 26, 267 (1986).

FIGURE CAPTIONS

FIG. 1. Coordinate systems: (a) Toroidal coordinates for a tokamak plasma; (b) Velocity space coordinates showing the trapping region for particles at $R = R_1$.

FIG. 2. Projection of a trapped particle orbit in a rotating plasma on the r-θ plane: (a) Plasma rotating with co-beam injection; (b) Plasma rotating with counter-beam injection.

FIG. 3. First banana orbit of a freshly ionized impurity ion in a rotating plasma: (a) Plasma rotating with co-beam injection; (b) Plasma rotating with counter-beam injection.

FIG. 4. Orbit characteristics of a particle trapped between fixed poloidal angles in a rotating plasma: (a) Variation of banana width with rotation frequency; (b) Variation of bounce frequency with rotation frequency. The initial conditions are: $r = 0.4$ m, $\theta = 1.6$ radians, $v_{\parallel} = 0$, $v_{\perp} = 9.1 \times 10^4$ m/s.

FIG. 5. Orbit characteristics of a trapped particle with fixed velocity at $\theta = 0$: (a) Variation of banana width with rotation frequency; (b) Variation of bounce frequency with rotation frequency. The initial conditions are: $r = 0.4$ m, $\theta = 0$, $v_{\parallel} = 3.2 \times 10^4$ m/s, $v_{\perp} = 4.6 \times 10^4$ m/s. It becomes a passing particle at $\omega = 0$.

FIG. 6. Schematic illustration of plasma rotation effects on the particle diffusion coefficient.

FIG. 7. Guiding center positions of 1024 particles: (a) At t = 0; (b) At t = 0.41 ms.

FIG. 8. Variation of Δ^2 with time.

FIG. 9. Comparison of calculated diffusion coefficients in a rotating plasma and a stationary plasma.

FIG. 10. Variation of diffusion coefficient (at r = a/2) with plasma current at two rotation frequencies.

FIG. 11. Variation of diffusion coefficient in a rotating plasma with collision frequency.

FIG. 12. Variation of diffusion coefficient in a rotating plasma with rotation velocity.

FIG. 13. Guiding center positions of 3072 particles near the edge of a rotating plasma: (a) t = 0; (b) t = 4.92 ms in a rotating plasma; (c) t = 4.92 ms in counter-rotating plasma.

FIG. 14. Guiding center positions of 1024 particles in a collisional rotating plasma: (a) t = 0; (b) t = 0.246 ms. The collision frequency is 100 times higher than the case shown in Fig. 7 and the rotation velocity is two times higher.

FIG. 15. Comparison of particle loss rates in co-rotating and counter-rotating plasmas. N is the number of remaining particles.

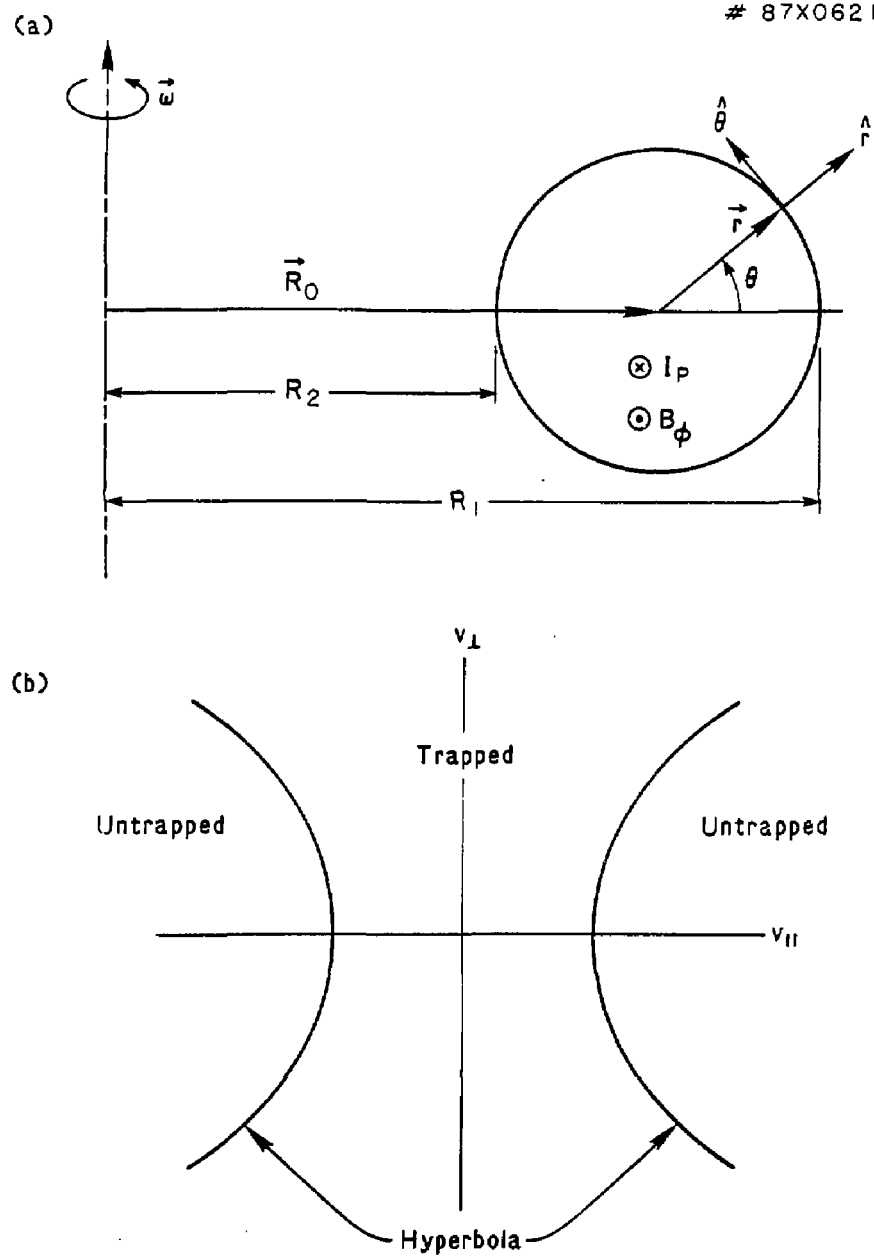
(a)
$\vec{\omega}$
$\hat{\theta}$
$\hat{r}$
$\vec{r}$
θ
$\vec{R}_0$
R_2
$\otimes I_p$
$\odot B_\phi$
R_1
(b)
$v_\perp$
Trapped
Untrapped
Untrapped
$v_{||}$
Hyperbola

Fig. 1

#87X0712

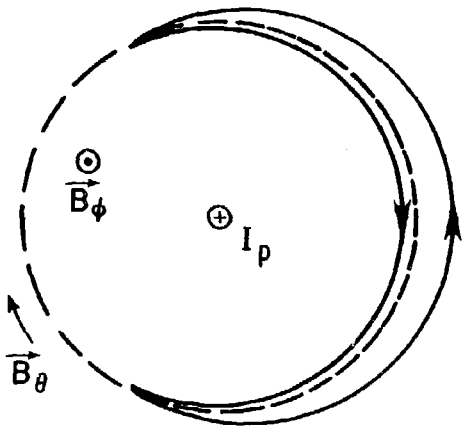

(a) CO-INJECTION

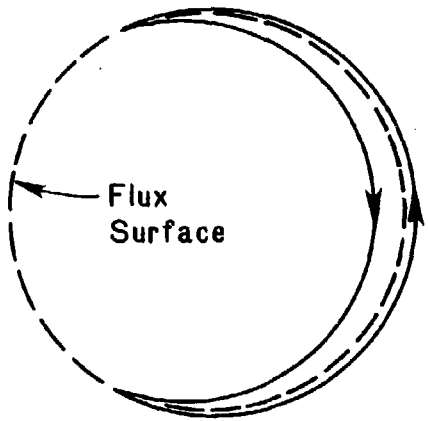

(b) COUNTER-INJECTION

Fig. 2

#87X0329

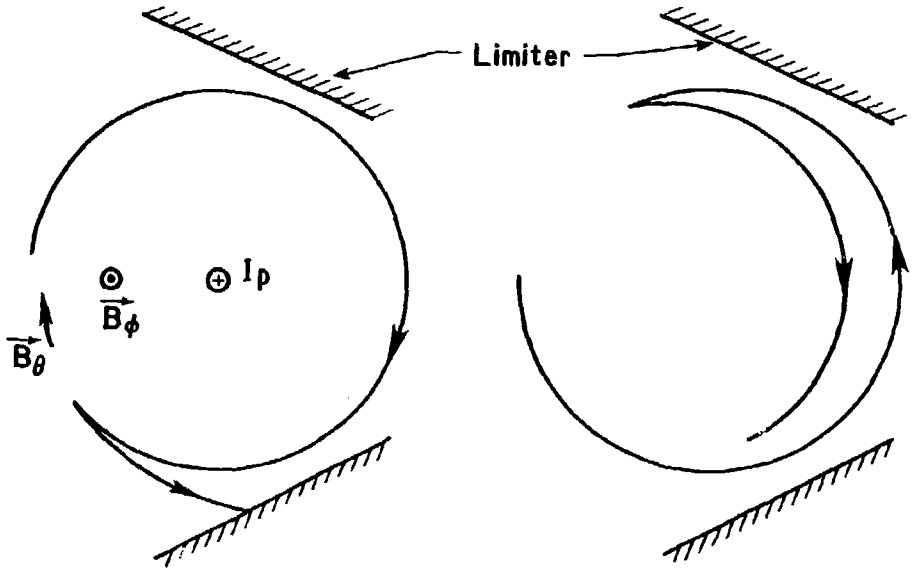

Fig. 3

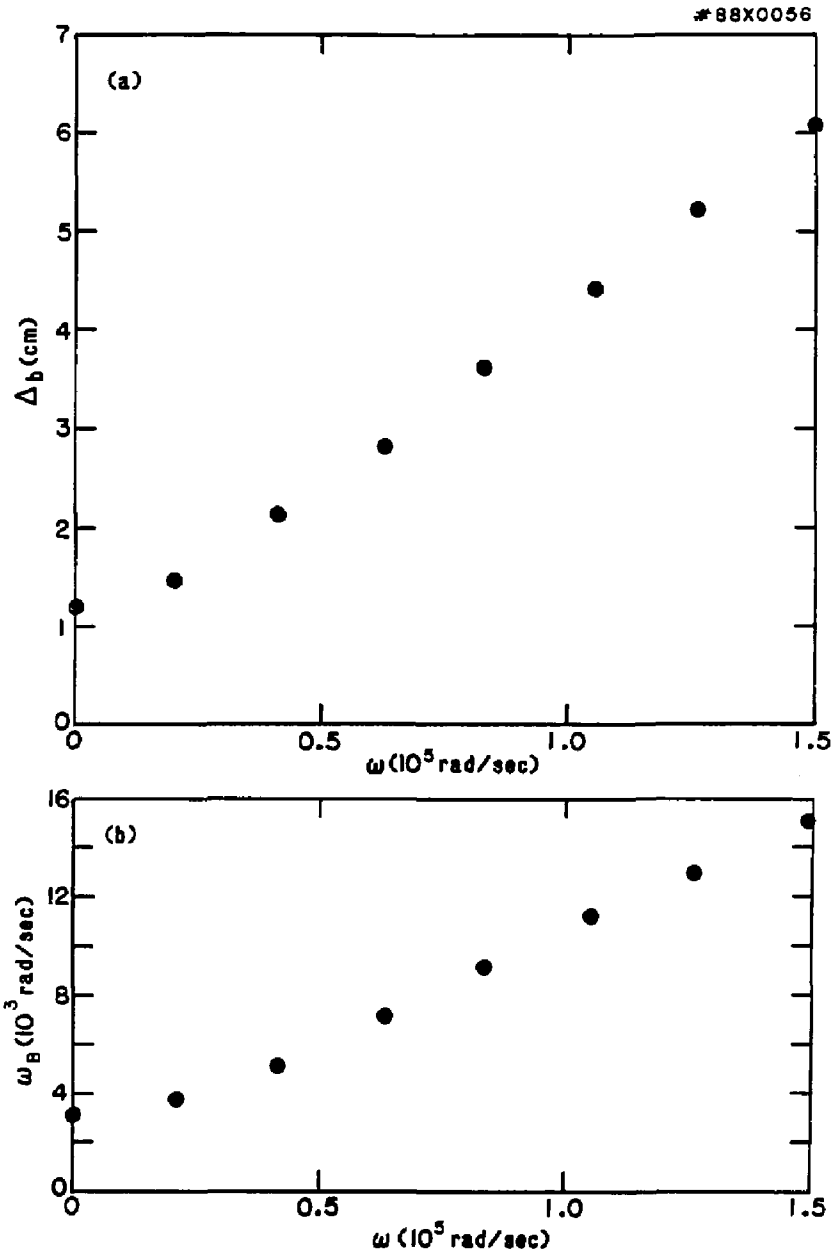
#88X0056
(a)
Δ_b (cm)
ω (10^5 rad/sec)
(b)
ω_B (10^3 rad/sec)
ω (10^5 rad/sec)

Fig. 4

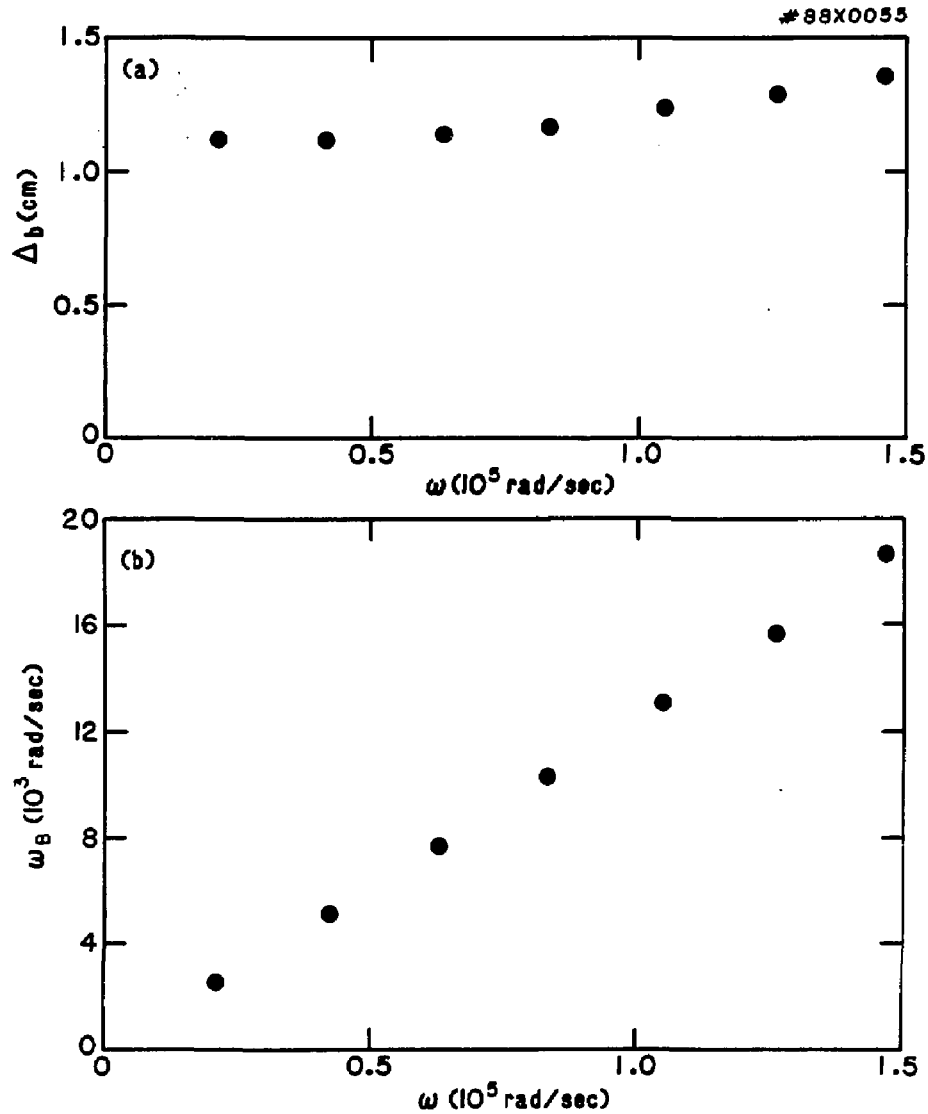
#88X0055
(a)
Δ_b (cm)
1.5
1.0
0.5
0
0
0.5
1.0
1.5
ω (10^5 rad/sec)
(b)
ω_B (10^3 rad/sec)
20
16
12
8
4
0
0
0.5
1.0
1.5
ω (10^5 rad/sec)

Fig. 5

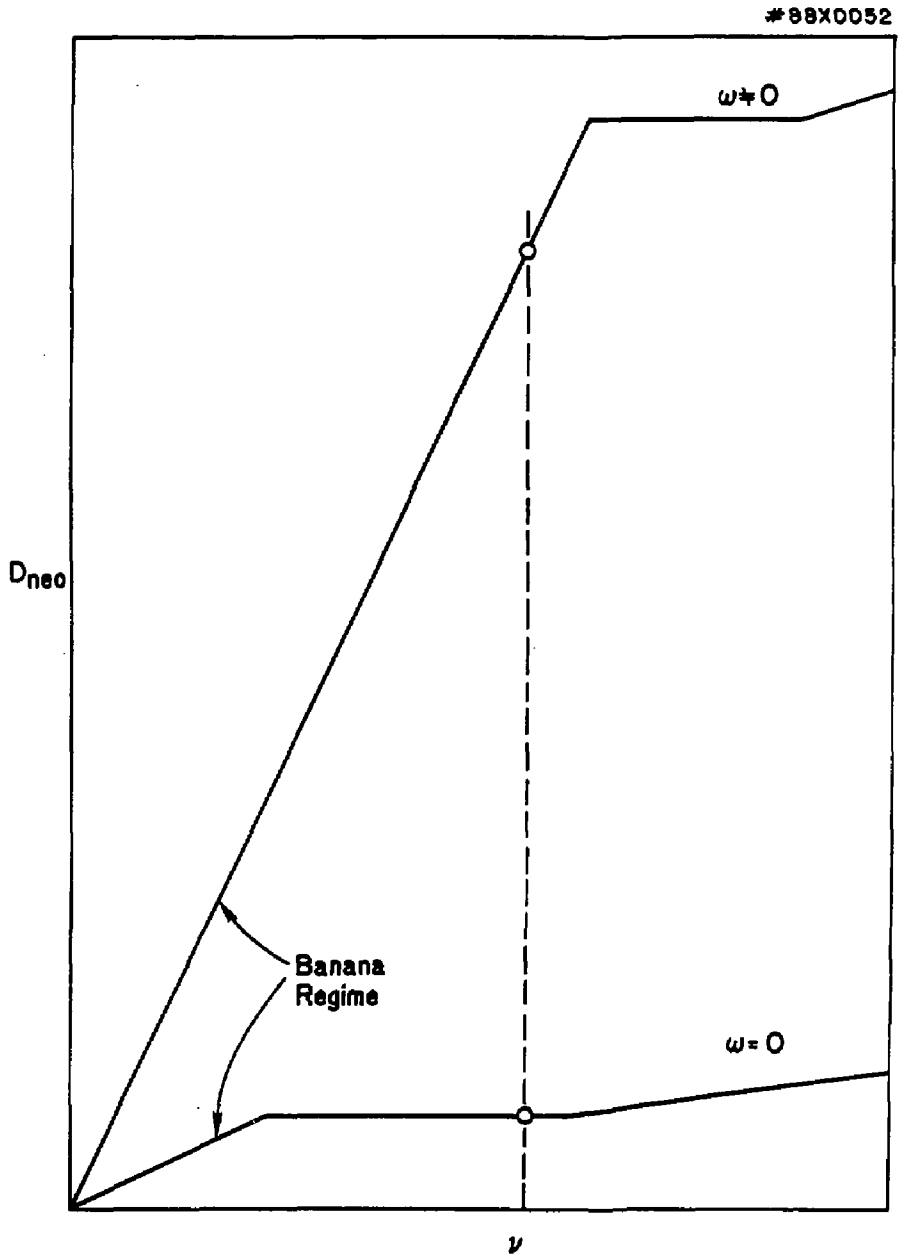

Fig. 6

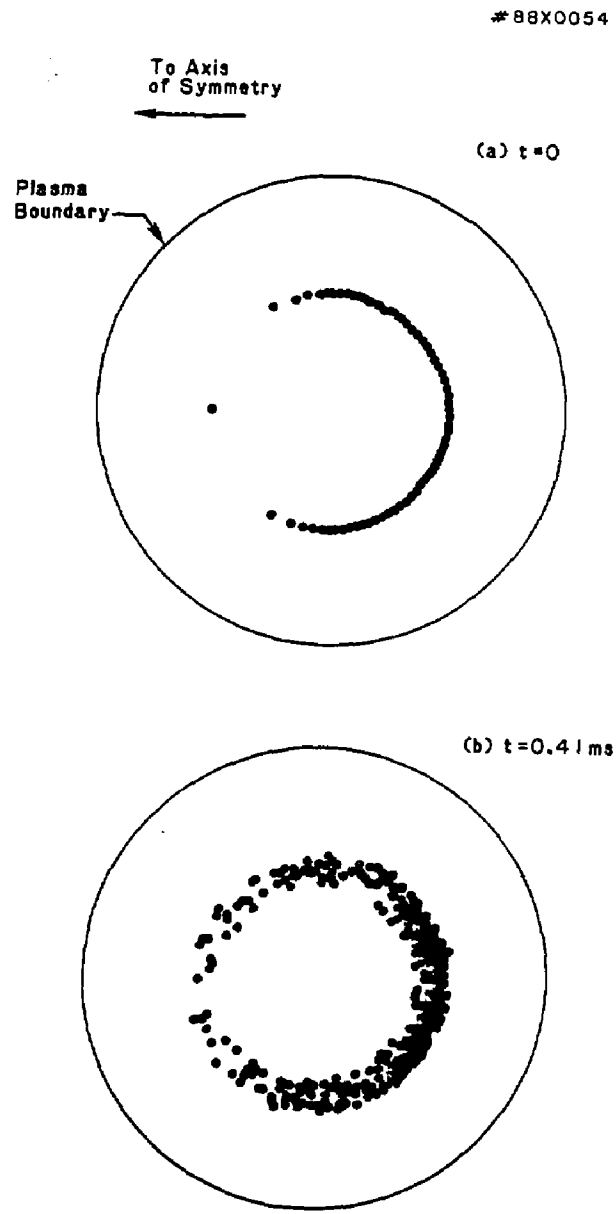

Fig. 7

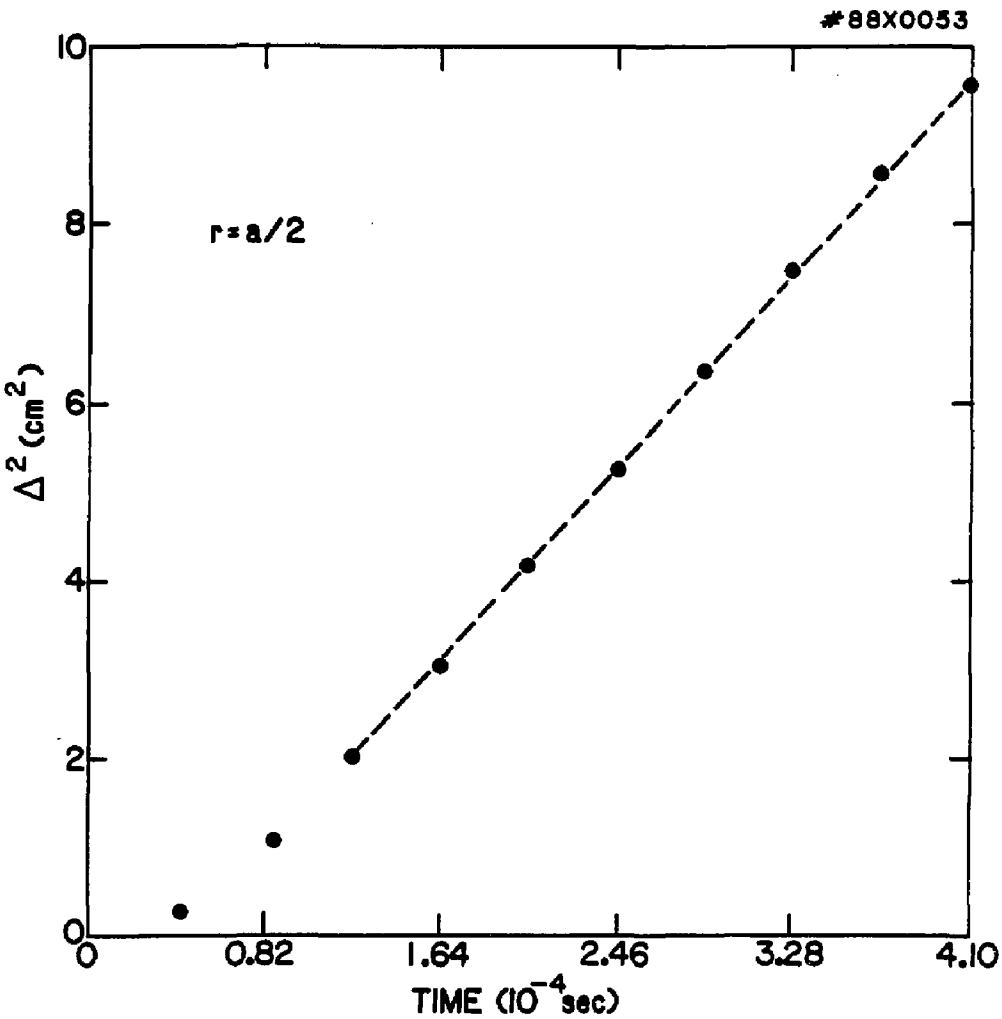
#88X0053
r=a/2
Δ^2 (cm^2)
TIME (10^{-4} sec)
0
2
4
6
8
10
0
0.82
1.64
2.46
3.28
4.10

Fig. 8

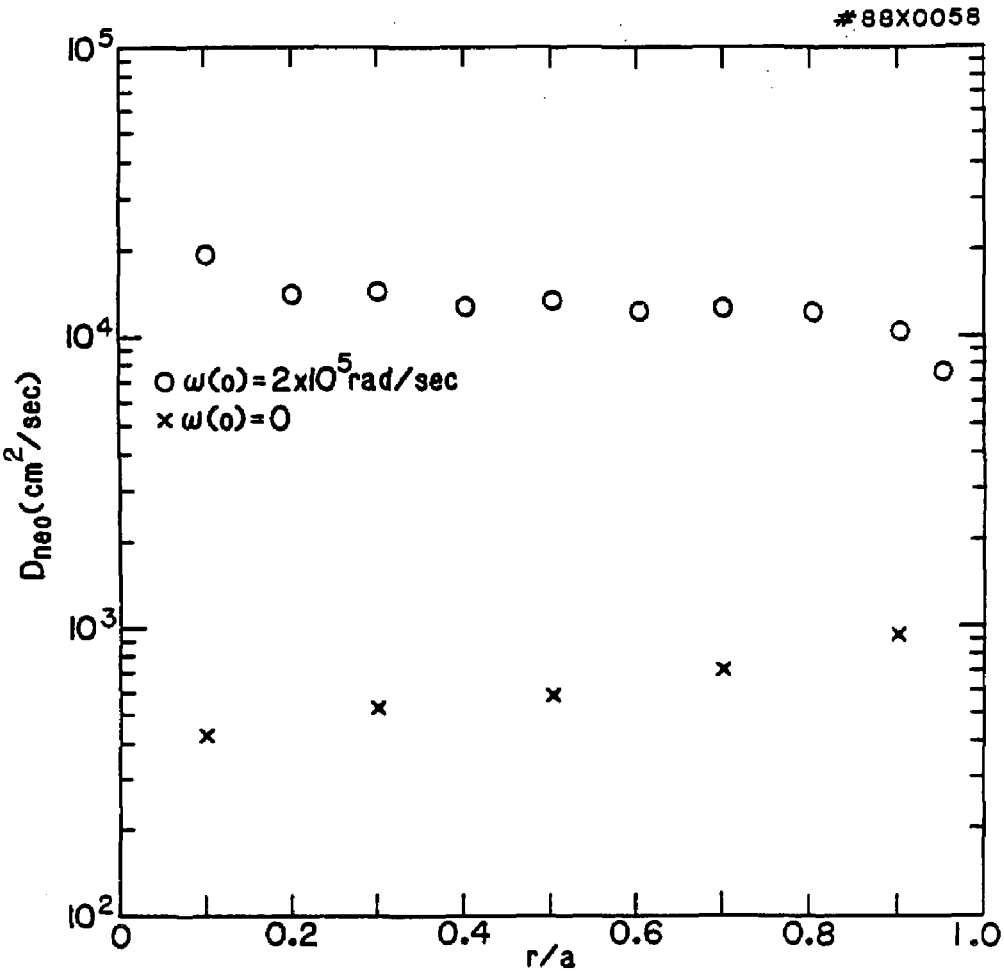
#88X0058
10^5
10^4
10^3
10^2
$D_{neo}(cm^2/sec)$
o ω(o)=2x10^{5}rad/sec
x ω(o)=0
0
0.2
0.4
0.6
0.8
1.0
r/a

Fig. 9

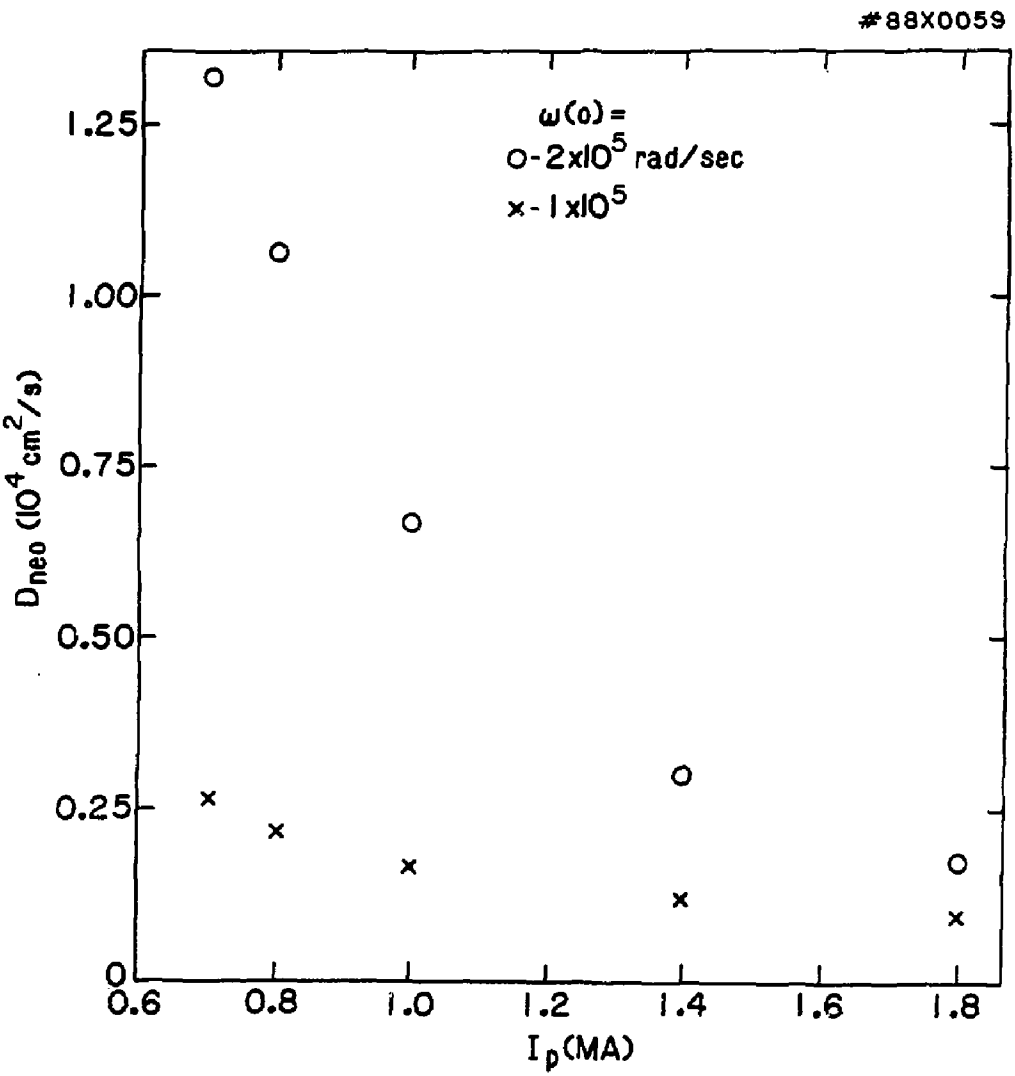
#88X0059
ω(o) =
o - 2x10^5 rad/sec
x - 1x10^5
1.25
1.00
0.75
0.50
0.25
0
D_neo (10^4 cm^2/s)
0.6
0.8
1.0
1.2
1.4
1.6
1.8
I_p (MA)

Fig. 10

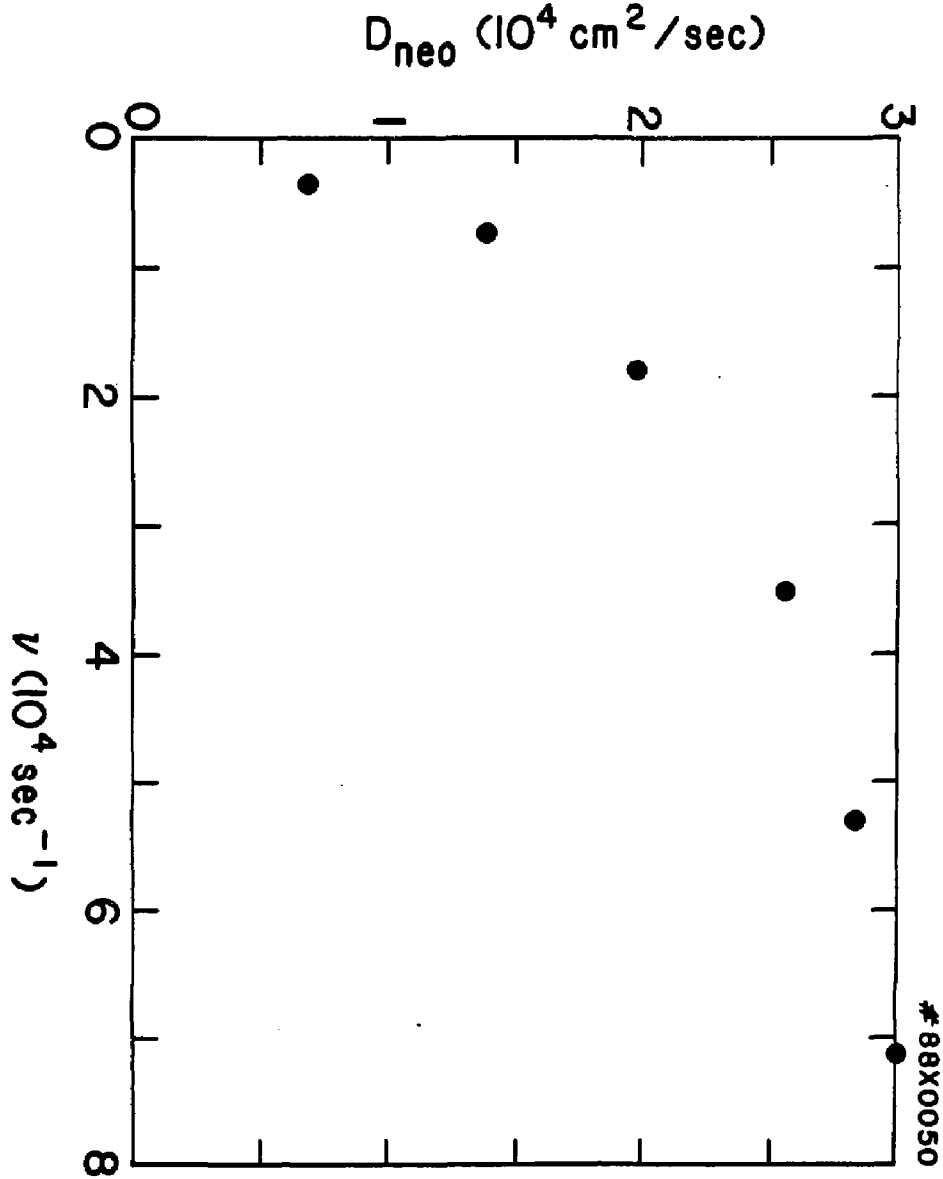

Fig. 11

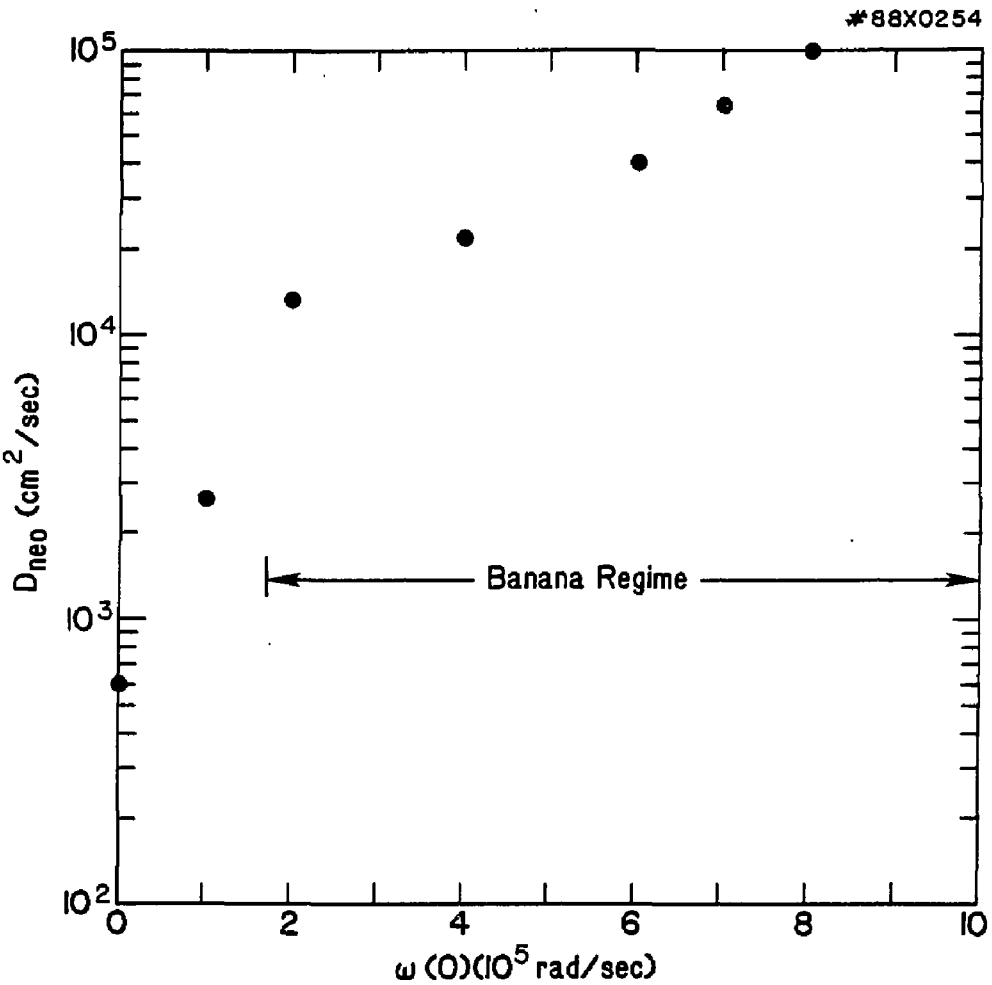
#88X0254
10^5
10^4
10^3
10^2
D_{neo} (cm^2/sec)
Banana Regime
0
2
4
6
8
10
ω (0)(10^5 rad/sec)

Fig. 12

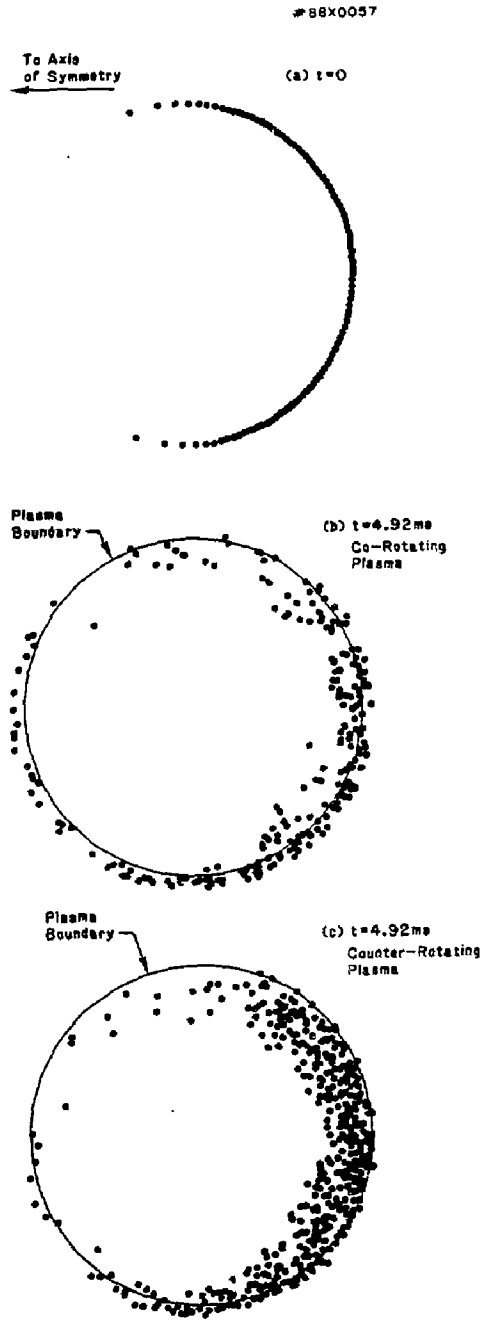
#88X0057
To Axis
of Symmetry
(a) t=0
Plasma
Boundary
(b) t=4.92ms
Co-Rotating
Plasma
Plasma
Boundary
(c) t=4.92ms
Counter-Rotating
Plasma

Fig. 13

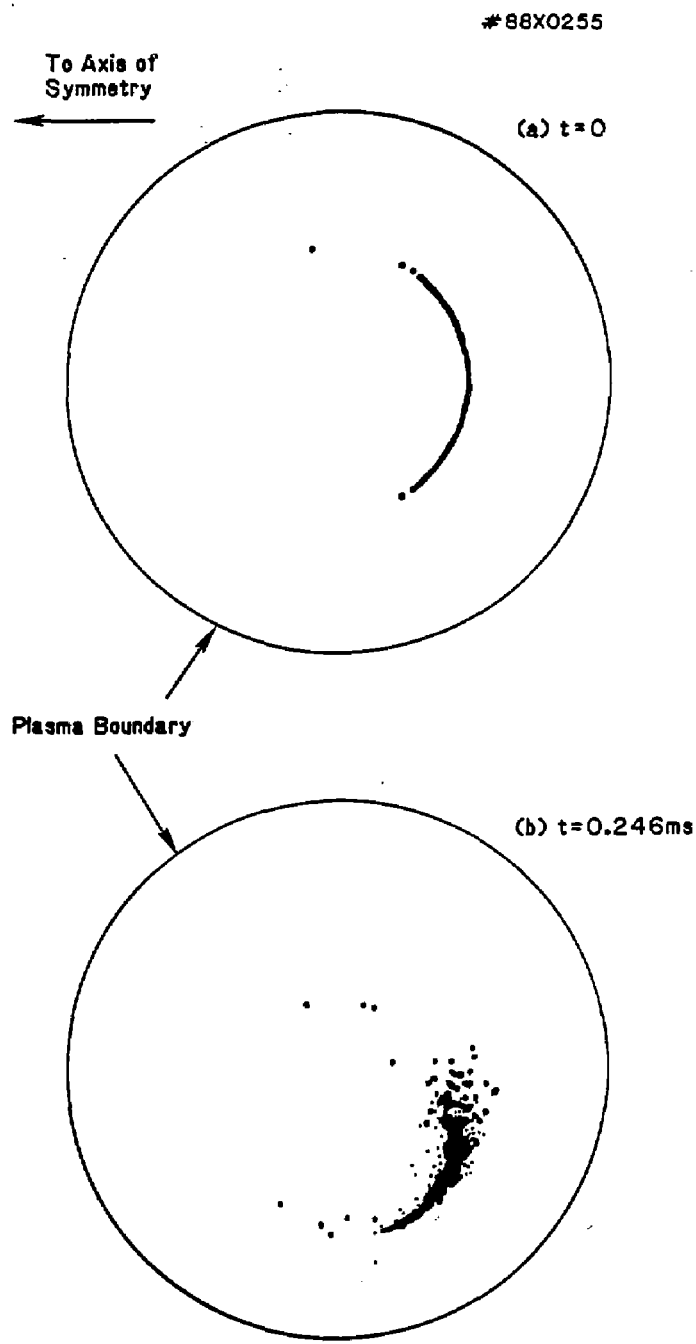

Fig. 14

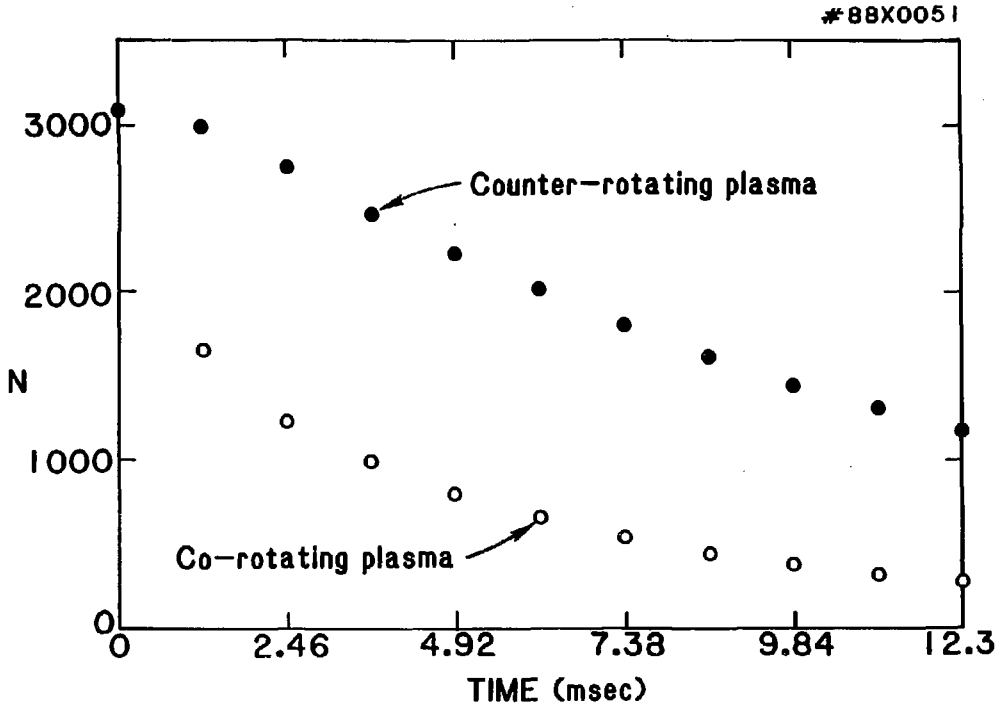
#88X0051
3000
2000
1000
0
N
Counter–rotating plasma
Co–rotating plasma
0
2.46
4.92
7.38
9.84
12.3
TIME (msec)

Fig. 15

EXTERNAL DISTRIBUTION IN ADDITION TO UC-20

Dr. Frank J. Paoloni, Univ of Wollongong, AUSTRALIA
Prof. M.H. Brennan, Univ Sydney, AUSTRALIA
Plasma Research Lab., Australian Nat. Univ., AUSTRALIA
Prof. I.R. Jones, Flinders Univ., AUSTRALIA
Prof. F. Cap, Inst Theo Phys, AUSTRIA
Prof. M. Heindler, Institut fur Theoretische Physik, AUSTRIA
M. Goossens, Astronomisch Instituut, BELGIUM
Ecole Royale Militaire, Lab de Phys Plasmas, BELGIUM
Commission-European, Dg-XII Fusion Prog, BELGIUM
Prof. R. Boucique, Laboratorium voor Natuurkunde, BELGIUM
Dr. P.H. Sakanaka, Instituto Fisica, BRAZIL
Instituto De Pesquisas Espaciais-INPE, BRAZIL
Documents Office, Atomic Energy of Canada Limited, CANADA
Dr. M.P. Bachynski, MPB Technologies, Inc., CANADA
Dr. H.M. Skarsgard, University of Saskatchewan, CANADA
Dr. H. Barnard, University of British Columbia, CANADA
Prof. J. Teichmann, Univ. of Montreal, CANADA
Prof. S.R. Sreenivasan, University of Calgary, CANADA
Prof. Tudor W. Johnston, INRS-Energie, CANADA
Dr. C.R. James, Univ. of Alberta, CANADA
Dr. Peter Lukac, Komenskeho Univ, CZECHOSLOVAKIA
The Librarian, Culham Laboratory, ENGLAND
The Librarian, Rutherford Appleton Laboratory, ENGLAND
Mrs. S.A. Hutchinson, JET Library, ENGLAND
C. Mouttet, Lab. de Physique des Milieux Ionises, FRANCE
J. Radet, CEN/CADARACHE - Bat 506, FRANCE
Univ. of Ioannina, Library of Physics Dept. GREECE
Dr. Tom Mual, Academy Bibliographic Ser., HONG KONG
Preprint Library, Hungarian Academy of Sciences, HUNGARY
Dr. B. Dasgupta, Saha Inst of Nucl. Phys., INDIA
Dr. P. Kaw, Institute for Plasma Research, INDIA
Dr. Philip Rosenau, Israel Inst. Tech, ISRAEL
Librarian, Int'l Ctr Theo Phys, ITALY
Prof. G. Rostagni, Univ Di Padova, ITALY
Miss Clelia De Palo, Assoc EURATOM-ENEA, ITALY
Biblioteca, Instituto di Fisica del Plasma, ITALY
Dr. H. Yamato, Toshiba Res & Dev, JAPAN
Prof. I. Kawakami, Atomic Energy Res. Institute, JAPAN
Prof. Kyoji Nishikawa, Univ of Hiroshima, JAPAN
Direc. Dept. Large Tokamak Res. JAERI, JAPAN
Prof. Satoshi Itoh, Kyushu University, JAPAN
Research Info Center, Nagoya University, JAPAN
Prof. S. Tanaka, Kyoto University, JAPAN
Library, Kyoto University, JAPAN
Prof. Nobuyuki Inoue, University of Tokyo, JAPAN
S. Mori, JAERI, JAPAN
Librarian, Korea Advanced Energy Res. Institute, KOREA
Prof. D.I. Choi, Adv. Inst Sci & Tech, KOREA
Prof. B.S. Liley, University of Waikato, NEW ZEALAND
Institute of Plasma Physics, PEOPLE'S REPUBLIC OF CHINA
Librarian, Institute of Phys., PEOPLE'S REPUBLIC OF CHINA
Library, Tsing Hua University, PEOPLE'S REPUBLIC OF CHINA
Z. Li, Southwest Inst. Physics, PEOPLE'S REPUBLIC OF CHINA
Prof. J.A.C. Cabral, Inst Superior Tecnico, PORTUGAL
Dr. Octavian Petrus, AL I CUZA University, ROMANIA
Dr. Johan de Villiers, Fusion Studies, AEC, SO AFRICA
Prof. M.A. Hellberg, University of Natal, SO AFRICA
C.I.E.M.A.T., Fusion Div. Library, SPAIN
Dr. Lennart Stenflo, University of UMEA, SWEDEN
Library, Royal Inst Tech, SWEDEN
Prof. Hans Wilhelmson, Chalmers Univ Tech, SWEDEN
Centre Phys des Plasmas, Ecole Polytech Fed, SWITZERLAND
Bibliothaek, Fom-Inst Voor Plasma-Fysica, THE NETHERLANDS
Dr. D.D. Ryutov, Siberian Acad Sci, USSR
Dr. G.A. Eliseev, Kurchatov Institute, USSR
Dr. V.A. Glukhikh, Inst Electrophysical Apparatus, USSR
Dr. V.T. Tolok, Inst. Phys. Tech. USSR
Dr. L.M. Kovrizhnykh, Institute Gen. Physics, USSR
Nuclear Res. Establishment, Julich Ltd., W. GERMANY
Bibliothek, Inst. Fur Plasmaforschung, W. GERMANY
Dr. K. Schindler, Ruhr Universitat Bochum, W. GERMANY
ASDEX Reading Rm, IPP/Max-Planck-Institut fur Plasmaphysik, W. GERMANY
Librarian, Max-Planck Institut, W. GERMANY
Prof. R.K. Janev, Inst Phys, YUGOSLAVIA